Chapter 6
Comparison of LEAP-UCD-2017 CPT Results

Trevor J. Carey, Andreas Gavras, and Bruce L. Kutter

Abstract A cone penetrometer was specifically designed for the LEAP project to provide an assessment of centrifuge model densities independent from mass and volume measurements. This paper presents the design of the CPT and analyses of the results. Due to uncertainty in the specifications about how to define zero depth of penetration, about 20% of the CPT profiles were corrected to produce more accurate results. The procedure for depth correction is explained. After these corrections, penetration resistances at the representative depths of 1.5, 2, 2.5, and 3 m (prototype depth) are correlated to the reported specimen dry densities by linear regression. Using the inverse form of the linear regression equations, the density of each specimen could be estimated from the penetration resistance. Kutter et al. (LEAP-UCD-2017 comparison of centrifuge test results. In Model Tests and Numerical Simulations of Liquefaction and Lateral Spreading: LEAP-UCD-2017, 2019b) found that the density determined from penetration resistance was a more reliable predictor of liquefaction behavior than the reported density itself. Finally, the centrifuge tests at different LEAP facilities modeled the same prototype in different containers using different length scale factors (1/20 to 1/44); thus the ratio of layer thickness to cone diameter was different in each experiment. It appears that the penetration resistances are noticeably affected by container width and, to a lesser extent, resistance is affected by the length scale factor.

6.1 Introduction

One of the challenges encountered during LEAP-GWU-2015 was independently assessing the achieved density of the centrifuge models (Kutter et al. 2017). Uncertainty in the calculated density from measurements of mass and volume is affected by irregular or bumpy surfaces produced by sand pluviation and limited precision of the load cells used to measure mass. Cone penetrometers (CPTs) were selected as an independent method to assess the achieved specimen density.

T. J. Carey (✉) · A. Gavras · B. L. Kutter
Department of Civil and Environmental Engineering, University of California, Davis, CA, USA
e-mail: TJCarey@ucdavis.edu

B. Kutter et al. (eds.), *Model Tests and Numerical Simulations of Liquefaction and Lateral Spreading*, https://doi.org/10.1007/978-3-030-22818-7_6

To eliminate variability that would be encountered by using different CPT designs at each centrifuge laboratory, a new CPT was designed with the goal that it will be low cost and not require specialty machining (Carey et al. 2018). Total cost for the device, including the load cell, is less than $2000 US. The devices were fabricated at a machine shop at UC Davis and distributed to each of the centrifuge laboratories.

Carey et al. (2018) discussed the design and calibration and provided a cross and direct comparison of results using the LEAP CPT. This paper will briefly review the design of the device and provide additional analysis of the results from the LEAP-UCD-2017 exercise. Using a linear regression and penetration resistance at mid-depth of the model, densities are estimated for each experiment. The apparent effects of centrifuge length scale factor and model container width on CPT penetration resistance are also discussed.

6.2 Design

The LEAP CPT, sketched in Fig. 6.1, is a 60-degree cone, 6 mm in diameter, and is fabricated from stock stainless steel materials. The device uses a rod, protected by a hollow sleeve to transmit tip forces to a load cell, eliminating the need for a costly submerged tip strain gauge bridge. The load cell and the hollow sleeve are attached to a rigid aluminum block, which allows for simultaneous advancement of both the rod and sleeve. Carey et al. (2018) calculated for a vertical effective stress of 100 kPa and a maximum allowable tip force of 900 N, the device could safely penetrate sand with a relative density of about 100% to a depth of 4 m prototype scale without yielding the cone rod in compression.

Located 100 mm behind the cone shoulder is a 20-degree taper that transitions the 6 mm diameter sleeve to 8 mm. The 8 mm section increases the ruggedness of the device, and the location of the taper was chosen to be sufficient to limit increases in overburden stress at the cone tip from bearing stress generated at the taper.

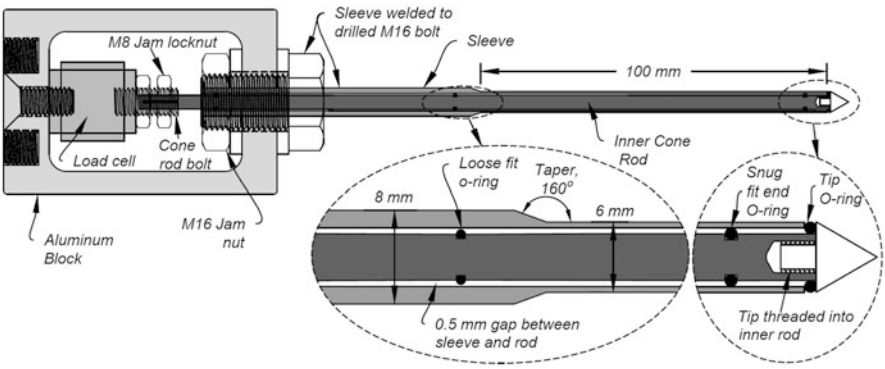

Fig. 6.1 Sketch of LEAP CPT from Carey et al. (2018)

The internal rod is solid stainless steel with a diameter of 4 mm. O-rings that have a diameter slightly smaller than the 5 mm inner diameter of the sleeve are spaced every 100 mm to reduce the unsupported length of the rod. The O-rings rest in grooves that are cut in the rod. Located just above the cone tip is a slightly larger tip O-ring with a 4 mm inner diameter and 1 mm cross section to prevent sand from filling the gap between the rod and sleeve. Preloading the tip O-ring is performed using a procedure described by Carey et al. (2018).

Carey et al. (2018) performed a series of calibration experiments to test (1) load transfer from the tip O-ring into the sleeve, (2) the influence of lateral force on cone tip forces, and (3) cycling loading to check if the internal O-rings had changing hysteresis during repeat cycles of loading. The load transfer from the tip O-ring to the sleeve under full design load was roughly 3% of the applied load; this effect is accounted for in the calibration of the cone. Tests confirm that the load cell was insensitive to inadvertent lateral loading of the cone. During cyclic loading hysteresis was observed, but following the first cycle of loading and unloading, additional cycles followed the same hysteresis as the prior cycle; the width of the hysteresis curve suggests that the magnitude of error due to hysteresis would correspond to less than 31 kPa of tip resistance, which is about 1.1% of the average tip resistance at mid-depth of the LEAP experiments.

6.3 LEAP-UCD-2017 Experiment

The specifications for the LEAP-UCD-2017 experiment are presented by Kutter et al. (2019a). The experiment consists of a uniform profile of Ottawa F-65 sand, inclined at 5 degrees in a rigid container. Test geometry, sensor layout, and prototype dimensions for the experiment are shown in Fig. 6.2. Twenty-four experiments were

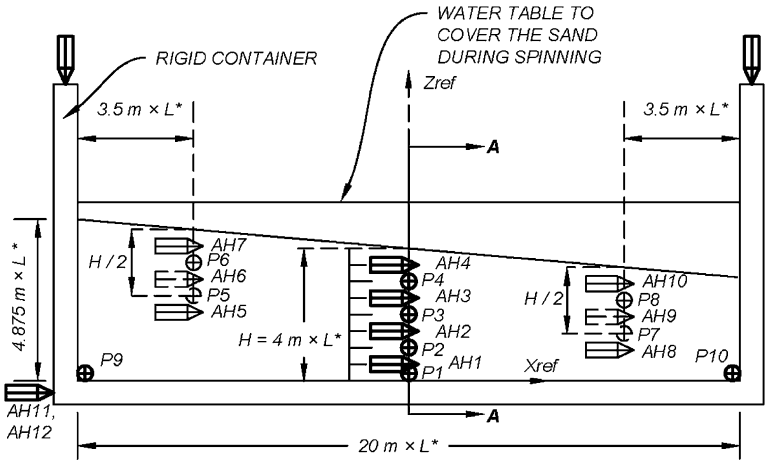

Fig. 6.2 Test geometry, sensor layout, and prototype dimensions of the LEAP-UCD-2017 experiment

conducted at nine participating facilities (National Central University (Taiwan), Zhejiang University (China), Kyoto University, University of Cambridge, IFSTTAR, UC Daivs, Ehime University, KAIST, Rensselaer Polytechnic Institute). The goal of the LEAP-UCD-2017 exercise was to perform experiments with relative densities ranging from about 50% (about 1599 kg/m^3) to about 80% (1703 kg/m^3) to determine the sensitivity of the model response to initial relative density.

6.4 Depth at Which the Cone Tip Touches the Surface (Depth of Zero Penetration)

When comparing results from different centrifuge tests, it is critical that the effective depth of the cone be consistently defined. A two-step process was used to determine the effective depth: (1) determine the depth of zero penetration and (2) adjust the depth to the 2/3 point on the cone tip. This section describes the first step in this process. Identifying when the tip of the cone touches the ground surface is complicated because the penetration resistance near the surface is very small and the surface area of the point of the cone tip is zero. Recognizing the complications in rectifying the point of zero penetration, the preferred practice was to accurately advance the tip of the cone to the sand surface before spinning the centrifuge. Unfortunately, some of the LEAP-UCD-2017 tests did not begin this way.

The proposed criteria compare the recorded penetration resistance (q_c) when the conical tip is just embedded into the soil with the ultimate bearing capacity (q_{bL}) of an equivalent prototype area square footing. It is assumed that the equivalent square footing will apply a similar magnitude of stress to the soil as would a fully embedded conical tip. Shown in Fig. 6.3 is an illustration of the point at which the conical tip is just embedded and an equivalent square footing. The bearing stress, $q_{bL,}$ of the square footing was determined to be 0.1 MPa for a dry density of 1668 kg/m^3, the median target density for the LEAP-UCD-2017 experiment. It was assumed that the depth at which the penetration resistance is 0.1 MPa corresponded approximately to the depth at which the conical tip is just embedded as shown in Fig. 6.3.

The different initial densities of the centrifuge models result in different penetration resistances at the stage depicted in Fig. 6.3. Therefore, when the recorded penetration resistance at full embedment of the conical tip was measured between $0.05 \leq q_c \leq 0.2$ MPa, it was deemed that no adjustment to the point of zero penetration (the location at which the point of the cone touches the surface) was

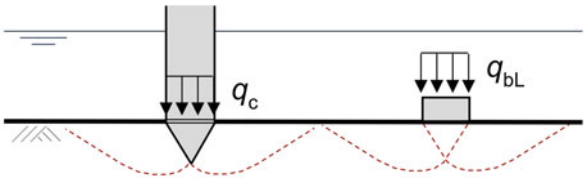

Fig. 6.3 Conical tip just embedded into the soil and equivalent area square surface footing

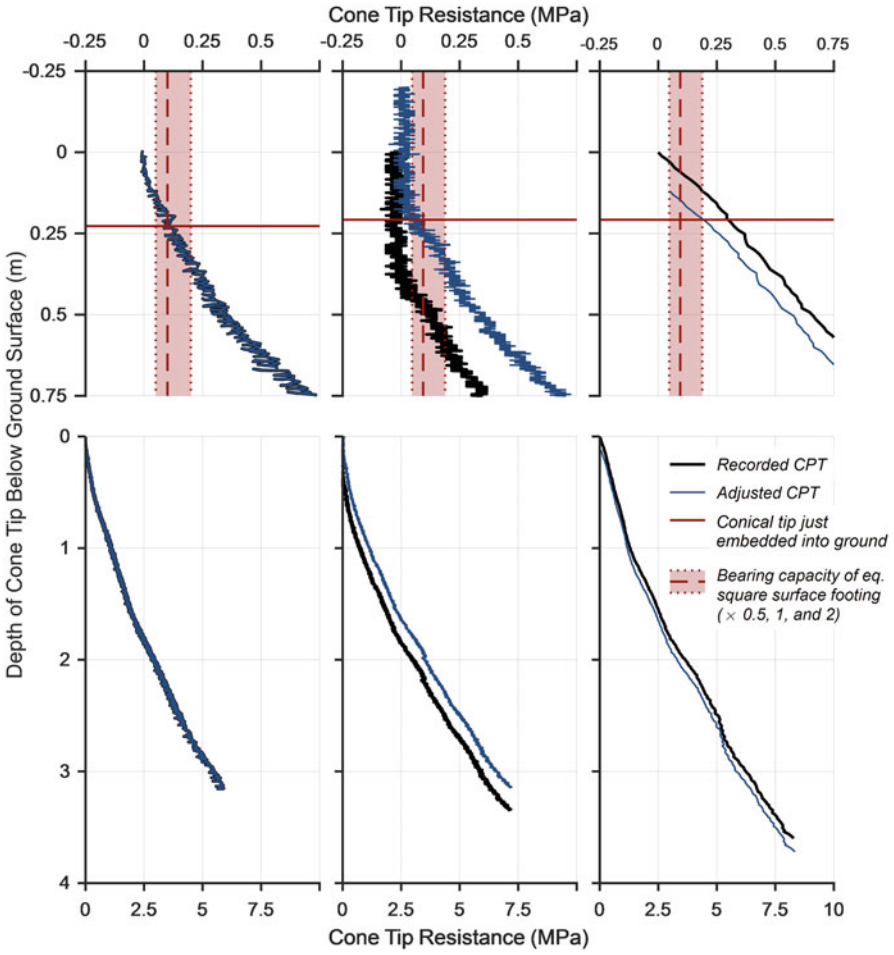

Fig. 6.4 Examples of CPT profiles were (1) No adjustment was needed; (2) Adjustment I, CPT started above ground surface; and (3) Adjustment II, CPT started embedded in ground surface

required. Roughly 80% of the CPT profiles did not require depth correction by these criteria. If the penetration resistance was $q_c < 0.05$ MPa, the "real" point of zero penetration is located above the reported depth = 0. The depth of the point of zero penetration is then corrected by shifting the data upward by the prototype length of the conical tip ((3 mm)/(tan 30°) × length scale factor) from where q_c is equal to 0.1 MPa. This scenario is referred to as Adjustment I and was applied to about 12% of the CPT soundings. If the reported point of zero penetration is located too far below the actual soil surface, $q_c > 0.2$ MPa. For this case, called Adjustment II, the point of zero penetration is shifted downward until q_c is equal to 0.1 MPa. Figure 6.4 provides examples of a CPT sounding where adjustment was not required and soundings adjusted in accordance with Adjustment I and II.

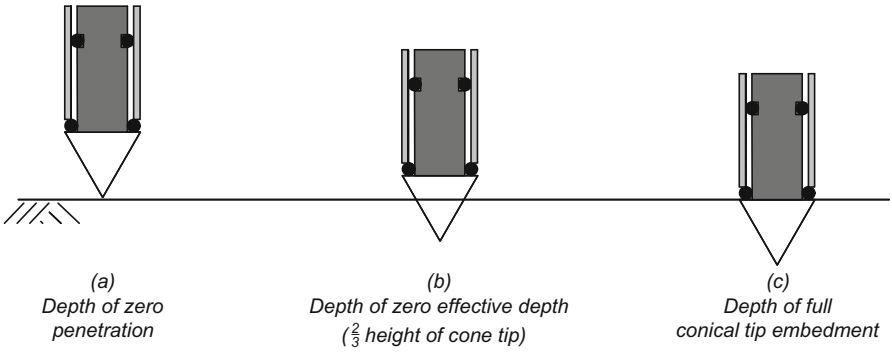

Fig. 6.5 Definition of different reference depths. (**a**) Depth of zero penetration (tip located at group surface), (**b**) depth corresponding to zero effective depth (2/3 height of the cone tip), (**c**) depth at which the conical tip is fully embedded

After the correct points of zero penetration (the locations where the point of the cone tip touches the ground) were determined, all soundings were adjusted so the effective depth of the cone tip corresponded to the 2/3 point of the cone tip height (2/3)(5.19 mm), which is consistent with industry practice. Figure 6.5 shows the point at which the effective depth (z) of the cone tip is considered to be zero.

Eleven CPT devices were manufactured at the University of California Davis and shipped to seven of the centrifuge facilities. The University of Cambridge used their own cone design, which Carey et al. (2018) showed produced comparable penetration resistances as the LEAP design. Shown in Fig. 6.6 are all 59 CPT soundings and reported dry densities for each experiment. CPT measurements were performed prior to shaking for assessment of specimen density. Additional CPTs were performed prior to each destructive motion (i.e., second and third).

For interpretation of the CPT data, penetration tip resistances at representative depths of 1.5, 2.0, 2.5, and 3.0 m prototype were considered. In Fig. 6.7, the penetration resistances at the representative depths are plotted against the density reported from mass and volume measurements of the model specimen. General trends of increasing cone tip stress with depth and initial dry density can be observed. The red solid line is a linear mean regression, and the blue dashed lines are the 95% confidence interval of the linear fit. The confidence intervals become wider at the 2.5 and 3.0 m depths due to (1) larger variance in the data and (2) increased standard error from fewer data points. (Not all facilities were able to push to 2.5 and 3.0 m depths.)

The linear trend, with the form $q_c = a \cdot \rho_d + b$, has depth-dependent coefficients a and b, which are provided in Table 6.1. With the inverse trend, $\rho_d = (q_c - b)/a$, the specimen density can be estimated from the penetration resistance, an alternative assessment of the reported densities.

Shown in Fig. 6.8 is an example of the density correction for points to the left and right of the trend line at 2.0 m depth. As an example, the experiment to the right of

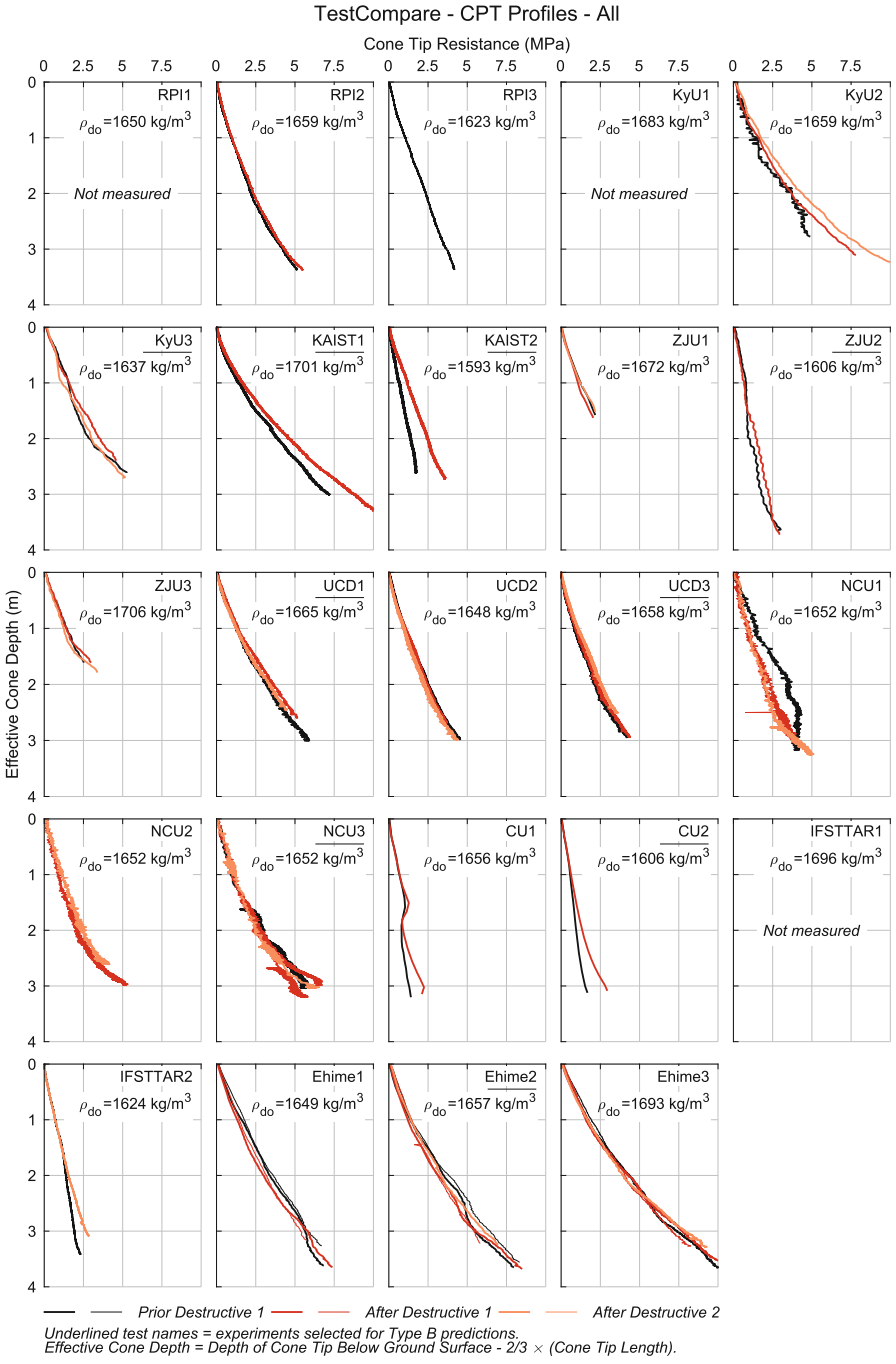

Fig. 6.6 All CPT profiles for LEAP-UCD-2017

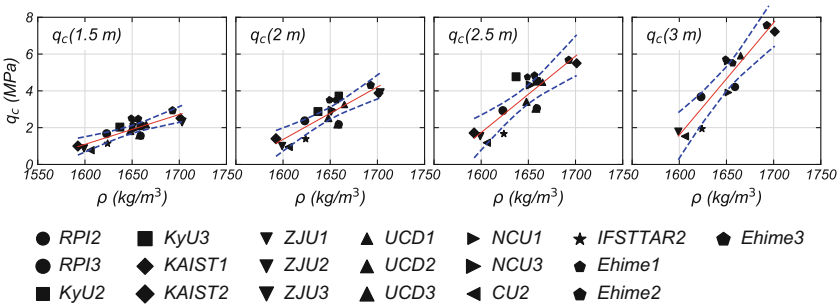

Fig. 6.7 Penetration resistances at 1.5, 2.0, 2.5, and 3.0 m depths vs. reported specimen density. The red solid lines are the linear mean regressions fit, and the blue dashed lines are the 95% confidence interval of the linear fit

Table 6.1 Coefficients of the linear trend lines ($q_c = a \cdot \rho_d + b$) for depths 1.5, 2.0, 2.5, and 3 m shown in Fig. 6.7

Depth (m)	A	B
1.5	0.0163	−24.9
2.0	0.0285	−44.3
2.5	0.0416	−64.8
3.0	0.0611	−96.1

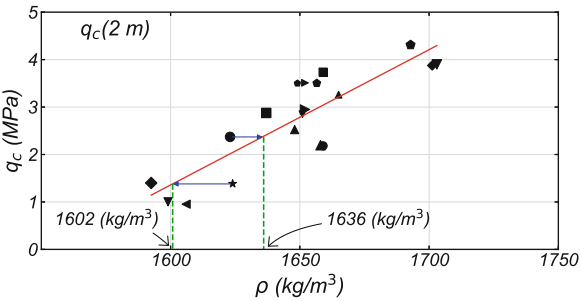

Fig. 6.8 Density corrected using the linear trend at 2 m depth and penetration resistance

the line has a reported density of 1624 kg/m^3 and a penetration resistance of 1.38 MPa. When that point is corrected back to the trendline, the density decreases to 1602 kg/m^3. Kutter et al. (2019b) showed that at 2.0 m depth, densities determined from penetration resistances better correlate with liquefaction performance measurements than densities from mass and volume measurements.

Tabulated in Table 6.2 are the reported dry densities from mass and volume and densities calculated from the linear regression and penetration resistance. Relative densities of the mass and volume density measurements are also provided in Table 6.2 ($\rho_{min} = 1490.5$ kg/m^3 and $\rho_{max} = 1757.0$ kg/m^3 from Carey et al. 2019).

Table 6.2 Reported dry density, relative density, cone penetration resistances at 2 m depth, and density using linear regression and penetration resistance at 2 m depth (NT = no CPT data available)

Test ID	Dry density from mass and volume (kg/m^3)	Relative density from mass and volume (%)	Cone tip stress at 2 m depth q_c(2 m) (MPa)	Dry density from cone tip stress at 2.0 m depth $\rho(q_c(2))$ (kg/m^3)
CU1	1656	66	0.81	1581
CU2	1606	47	0.95	1586
Ehime1	1649	63	3.50	1676
Ehime2	1657	66	3.50	1676
Ehime3	1693	79	4.31	1704
IFSTTAR1	1696	80	NT	NT
IFSTTAR2	1624	56	1.38	1602
KAIST1	1701	82	3.88	1689
KAIST2	1593	42	1.40	1602
KyU1	1683	75	NT	NT
KyU2	1659	67	3.74	1684
KyU3	1637	59	2.88	1654
NCU1	1652	64	3.51	1676
NCU2	1652	64	NT	NT
NCU3	1652	64	2.95	1656
RPI1	1650	64	NT	NT
RPI2	1659	67	2.18	1630
RPI3	1623	54	2.37	1636
UCD1	1665	69	3.26	1667
UCD2	1648	63	2.52	1642
UCD3	1658	67	2.19	1630
ZJU1	1651	64	2.85	1653
ZJU2	1599	45	1.00	1588
ZJU3	1703	82	3.90	1690

6.5 Effects of Scale Factor and Container Width

Since each facility used the same 6 mm diameter cone in model scale, the prototype size of the cone varied from 138 mm (RPI) to 300 mm (IFSTTAR). Bolton et al. (1999) demonstrated that if the normalized penetration depth to CPT diameter ratio was greater than 10 for relative densities of 80%, then the normalized penetration is not sensitive to depth. At a 2 m prototype depth in the IFSTTAR experiment, the depth to diameter ratio is 2000 mm/300 mm = 6.7, which is less than 10; therefore, reductions in penetration resistance may be expected in this case. In addition, cone penetration resistance for dilatant sand in rigid containers is known to increase as container width decreases.

To investigate container size and length scale factor effects further, the data for penetration resistance at a depth of 2 m were sorted, color coded, and replotted as

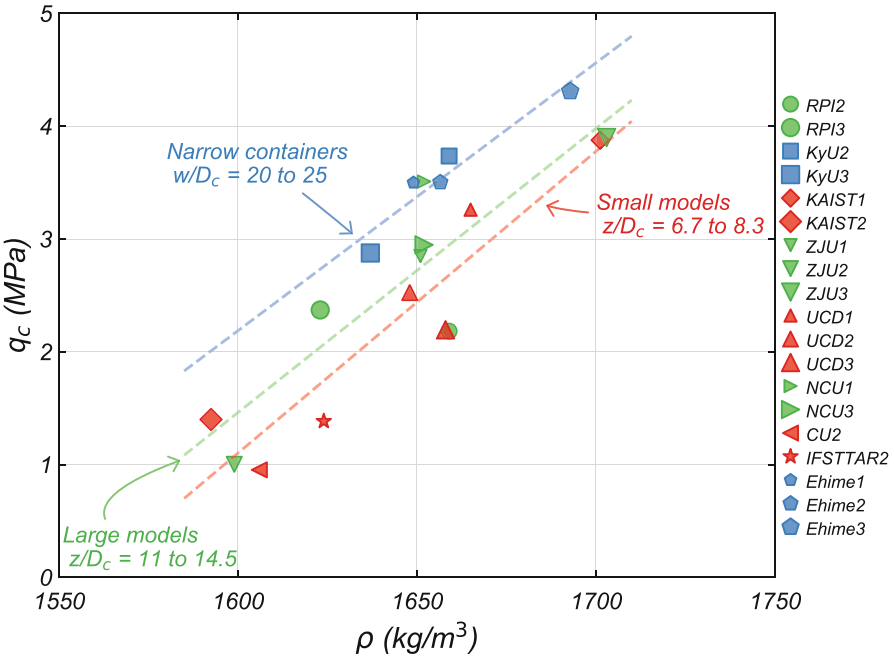

Fig. 6.9 Experiments are separated by (1) large models tested at lower centrifuge acceleration ($z/D_c = 11$ to 14.5) (green), (2) small models tested at high-g (z/Dc = 6.7 to 8.3) (red), and (3) narrow containers (w/Dc 20–25) (blue)

shown in Fig. 6.9. The experiments shown in green represent the larger models with wider containers tested at low g-levels (RPI, ZJU, and NCU). The number of normalized cone diameters (z/D_c = depth of interest/cone diameter) to $z = 2$ m for these experiments ranged from $z/D_c = 11$ to 14.5. Experiments represented by red points were the small models with wide containers tested at higher g-levels (KAIST, UCD, CU, and IFSTTAR); for these models, the ratio of depth to cone diameter at mid-depth of the model was only z/Dc = 6.7 to 8.3. Blue points represent experiments conducted in relatively narrow containers where the width of the container to cone diameter ratio was $w/D_c = 20$–25 (KyU, Ehime). For experiments other than KyU and Ehime, the container width ranged from w/Dc ≈ 33 to 67 cone diameters.

Linear regressions were computed for each group of data points; interestingly, these regressions defined the nearly parallel lines shown in Fig. 6.9. At a density of 1662 kg/m^3 (relative density of 68%), using the regressions for the large and small models, the predicted penetration resistances are 2.73 and 2.5 MPa, respectively, an 8% difference. Reduction in penetration resistances for the high-g experiments is consistent at 1.5 and 2.5 m depths where adequate data is available. Shown in Fig. 6.10 are the four color-coded depths of interest.

The experiments performed with narrow containers consistently have elevated penetration resistances. Bolton et al. (1999) showed that if the number of normalized

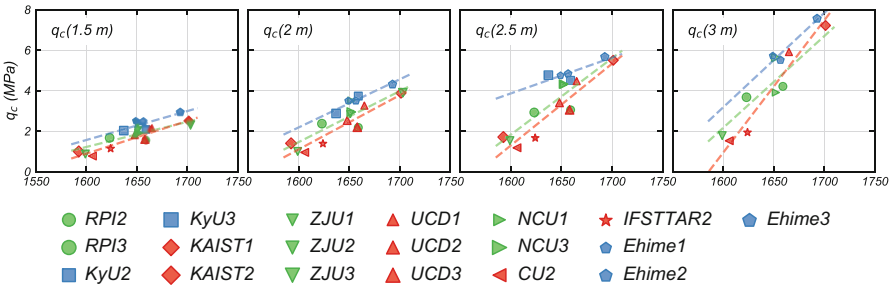

Fig. 6.10 Experiments are separated by (1) large models tested at lower centrifuge acceleration (green), (2) small models tested at high-g (red), and (3) narrow containers (blue) for each depth of interest. Note: data presented for 2 m depth is consistent with data presented in Fig. 6.9

cone diameters to the container boundary wall was less than 10, then the penetration resistance would increase. CPTs performed along the longitudinal centerline of the narrow containers would be roughly 10–12 normalized cone diameters from the boundary wall at the most. Using the narrow container linear regression, the predicted penetration resistance at a relative density of 68% is 3.37 MPa, 23% larger than the low-g experiments. The elevated penetration resistance for the narrow container experiments is expected to range from 10 to 25% for all relative densities.

Additional work is required to confirm the trends observed in Fig. 6.9, but the results are encouraging and are generally consistent with expectations based on correlations presented by Bolton et al. (1999). Much of the variance seen in the correlation depicted in Fig. 6.7 may be explained by container width and model size. Kutter et al. (2019b) showed however that the resistance to liquefaction is better characterized by the cone penetration resistance than it is by the measured mass and volume. It is possible that the effects of model size on penetration resistance somehow compensate the effects of model size on liquefaction resistance (i.e., perhaps q_c increases as container size decreases, and liquefaction resistance increases as container size increases.)

6.6 Conclusions

One of the challenges during LEAP-GWU-2015 was the lack of consistent measurements of the achieved specimen density. Using mass and volume to find density introduces uncertainty from both measurements; scales are typically only accurate to 0.1 kg, and point measurements of bumpy or irregular soil surfaces do not accurately represent the entire depth of soil. A low-cost CPT device was developed in an effort to maximize the likelihood of obtaining a useful correlation between penetration tests and density at different facilities. Carey et al. (2018) provides an overview of the design and calibration procedures.

Facilities reported their penetration tests as q_c vs. depth, but there was no guarantee that the cone tip started at the ground surface. A procedure was presented to evaluate when the cone tip just touches the ground surface using the recorded penetration resistance (q_c) and a reference ultimate bearing capacity from an equivalent area square footing. Furthermore, the effective depth (z) was adjusted for all CPT profiles so that depth = 0 when the conical tip is embedded to 2/3 of its length (2/3 of the distance from the point of the cone-to-cone shoulder).

Penetration resistances at depths of 1.5, 2.0, 2.5, and 3.0 m depths were plotted against specimen density, computed from mass and volume. Linear trend lines were computed for each depth. Inverse equations from the linear regression lines were used then to determine dry density from penetration resistance. Kutter et al. (2019b) showed the densities calculated from penetration resistance at 2.0 m depth were better correlated to liquefaction performance measures than densities from mass and volume.

Additional investigation was done to explore the effects of container width and scale factor on penetration resistance. Consistent with work from Bolton et al. (1999), systematic sensitivity to the normalized container width (w/Dc) and the normalized depth (z/Dc = depth/cone diameter) seems apparent. It was argued that the effect of w/Dc on penetration resistance might be similar to the effect of w/Dc on the liquefaction resistance. If this is so, then this might contribute to explain why liquefaction resistance is better correlated to penetration resistance than to reported densities.

Acknowledgments Funding for this work is supported by NSF under CMMI Grant Number 1635307. The authors would like to the thank each of the participating LEAP facilities for providing CPT data. Thank you, Kate Darby, for providing data during the initial design process. Barry Zheng's help during data processing was much appreciated. The authors would also like to thank Andy Cobb at UCD's BAE shop for providing construction recommendations and manufacturing each device.

References

Bolton, M. D., Gui, M. W., Garnier, J., Corte, J. F., Bagge, G., Laue, J., & Renzi, R. (1999). Centrifuge cone penetration tests in sand. *Geotechnique, 49*(4), 543–552.

Carey, T., Gavras, A., Kutter, B., Haigh, S. K., Madabhushi, S. P. G., Okamura, M., Kim, D. S., Ueda, K., Hung, W.-Y., Zhou, Y.-G., Liu, K., Chen, Y.-M., Zeghal, M., Abdoun, T., Escoffier, S., & Manzari, M. (2018). A new shared miniature cone penetrometer for centrifuge testing. In *Proceedings of 9th International Conference on Physical Modelling in Geotechnics, ICPMG 2018* (Vol. 1, pp. 293–229). London: CRC Press/Balkema.

Carey, T. J., Stone, N., & Kutter, B. L. (2019). Grain size analysis and maximum and minimum dry density testing of Ottawa F-65 sand for LEAP-UCD-2017. In B. Kutter et al. (Eds.), *Model tests and numerical simulations of liquefaction and lateral spreading: LEAP-UCD-2017*. New York: Springer.

Kutter, B. L., Carey, T. J., Bonab, M. H., Stone, N., Manzari, M., Zeghal, M., Escoffier, S., Haigh, S., Madabhushi, G., Hung, W., Kim, D., Kim, N., Okamura, M., Tobita, T., Ueda, K., & Zhou, Y. (2019a). LEAP UCD 2017 version 1.01 model specifications. In B. Kutter et al. (Eds.),

Model tests and numerical simulations of liquefaction and lateral spreading: LEAP-UCD-2017. New York: Springer.

Kutter, B. L., Carey, T., Stone, N., Zheng, B. L., Gavras, A., Manzari, M., Zeghal, M., Abdoun, T., Korre, E., Escoffier, S., Haigh, S., Madabhushi, G., Madabhushi, S. S. C, Hung, W.-Y., Liao, T.-W., Kim, D.-S., Kim, S.-N., Ha, J.-G., Kim, N. R., Okamura, M., Sjafuddin, A. N., Tobita, T., Ueda, K., Vargas, R., Zhou, Y.-G., & Liu, K. (2019b). LEAP-UCD-2017 comparison of centrifuge test results. In B. Kutter et al. (Eds.), *Model tests and numerical simulations of liquefaction and lateral spreading: LEAP-UCD-2017*. New York: Springer.

Kutter, B. L., Carey, T. J., Hashimoto, T., Zeghal, M., Abdoun, T., Kokkali, P., Madabhushi, S. P. G., Haigh, S. K., Burali d'Arezzo, F., Madabhushi, S. S. C., Hung, W.-Y., Lee, C.-J., Cheng, H.-C., Iai, S., Tobita, T., Ashino, T., Ren, J., Zhou, Y.-G., Chen, Y., Sun, Z.-B., & Manzari, M. T. (2017). LEAP-GWU-2015 experiment specifications, results, and comparisons. *International Journal of Soil Dynamics and Earthquake Engineering, Elsevier, 113*, 616. https://doi.org/10.1016/j.soildyn.2017.05.018.